Osteoblast-specific deficiency of ectonucleotide pyrophosphatase or phosphodiesterase-1 engenders insulin resistance in high-fat diet fed mice

Journal of Cellular Physiology

Osteoblast-specific deficiency of ectonucleotide pyrophosphatase/ phosphodiesterase-1 engenders insulin resistance in high-fat diet fed mice

Journal:	*Journal of Cellular Physiology*
Manuscript ID	JCP-20-0474.R3
Wiley - Manuscript type:	Original Research Article
Date Submitted by the Author:	14-Nov-2020
Complete List of Authors:	Roberts, Fiona ; The University of Edinburgh The Roslin Institute Rashdan, Nabil; The University of Edinburgh The Roslin Institute Phadwal, Kanchan; The University of Edinburgh The Roslin Institute; The University of Edinburgh The Roslin Institute, Functional Genetics and Development Markby, Greg; The University of Edinburgh The Roslin Institute Dillon, Scott; The University of Edinburgh The Roslin Institute Zoll, Janna; University of Hawai'i at Manoa John A Burns School of Medicine Berger, Julian; Columbia University Medical Center Milne, Elspeth; The University of Edinburgh The Roslin Institute Orriss, Isabel; Royal Veterinary College, Karsenty, Gerard; Columbia University Medical Center Saux, Olivier; University of Hawai'i at Manoa Morton, Nicholas; university of edinburgh Farquharson, Colin; University of Edinburgh, Division of Developmental Biology MacRae, Vicky; The Roslin Institute and Royal (Dick) School of Veterinary Studies , Division of Developmental Biology ;
Key Words:	Osteoblasts, Matrix mineralisation, Genetic animals models, Bone-fat interactions, non-collagenous proteins

Osteoblast-specific deficiency of ectonucleotide pyrophosphatase/ phosphodiesterase-1 engenders insulin resistance in high-fat diet fed mice

Short running title: **Osteoblast-specific metabolic actions of NPP1**

Authors:

Fiona L. Roberts[1*], Nabil A.Rashdan[1*], Kanchan Phadwal[1] , Greg R. Markby[1], Scott Dillon[1], Janna Zoll[2], Julian Berger[3], Elspeth Milne[1], Isabel R. Orriss[4], Gerard Karsenty[3], Olivier Le Saux[2], Nicholas M. Morton[5], Colin Farquharson[1], Vicky E MacRae[1].

* Both authors contributed equally to this work.

Author Affiliations:

1. The Royal (Dick) School of Veterinary Studies and The Roslin Institute, University of Edinburgh, Easter Bush Campus, Midlothian, EH25 9RG United Kingdom
2. John A. Burns School of Medicine, University of Hawaii at Manoa, 651 Ilalo St. Honolulu, HI, 98613, United States.
3. Department of Genetics and Development, Columbia University Medical Centre, 1602 HHSC, New York, NY, United States
4. Department of Comparative Biomedical Sciences, The Royal Veterinary College, Royal College Street, London, NW1 0TU, United Kingdom
5. University/British Heart Foundation Centre for Cardiovascular Science, The Queen's Medical Research Institute, The College of Medicine and Veterinary Medicine, The University of Edinburgh, 47 Little France Crescent, Edinburgh, EH16 4TJ.

Author contributions:

Conceived and designed the experiments: Fiona L Roberts, Nabil A Rashdan, Vicky E Macrae, Janna Zoll, Olivier Le Saux. Performed the experiments: Fiona L Roberts, Nabil A Rashdan, Greg R Markby, Scott Dillon, Julian Berger, Elspeth Milne, Isabel R Orriss. Analysed the Data: Fiona L Roberts, Isabel R Orriss, Elspeth Milne. Manuscript preparation: Fiona L Roberts. Manuscript revision: Fiona L Roberts, Nabil A Rashdan, Greg R Markby, Scott Dillon, Kanchan Phadwal, Janna Zoll, Julian Berger, Elspeth Milne, Isabel R Orriss, Gerard Karsenty, Olivier Le Saux, Nicholas M Morton, Colin Farquharson, Vicky E MacRae.

Funding and acknowledgments

This study was supported by funding from the Biotechnology and Biological Sciences Research Council (BBSRC) in the form of an Institute Strategic Programme Grant (BB/J004316/1;BBS/E/D/20221657) and International Partnering Award (BB/P02503X/1); British Heart Foundation (grant number PG/15/13/31296); pilot grant funding from Tenovus Scotland (E17/03) and R(D)VS PhD studentship funding.

Data availability statement

All the data that supports the findings of this study are available in main document and the supplementary material of this article.

Abstract

Supraphysiological levels of the osteoblast-enriched mineralisation regulator ectonucleotide pyrophosphatase/phosphodiesterase-1 (NPP1) is associated with type 2 diabetes mellitus. We determined the impact of osteoblast-specific Enpp1 ablation on skeletal structure and metabolic phenotype in mice.

Female, but not male, 6-week old mice lacking osteoblast NPP1 expression (osteoblast-specific KO) exhibited increased femoral bone volume/total volume (17.50% vs 11.67%; $p<0.01$), and reduced trabecular spacing (0.187mm vs 0.157mm; $P<0.01$) compared with floxed (control) mice. Furthermore, an enhanced ability of isolated osteoblasts from the osteoblast-specific KO to calcify their matrix *in vitro* compared to *fl/fl* osteoblasts was observed ($p<0.05$).

Male osteoblast-specific KO and *fl/fl* mice showed comparable glucose and insulin tolerance despite increased levels of insulin–sensitizing under-carboxylated osteocalcin (195% increase; $p<0.05$). However, following high-fat-diet challenge, osteoblast-specific KO mice showed impaired glucose and insulin tolerance compared with *fl/fl* mice.

These data highlight a crucial local role for osteoblast NPP1 in skeletal development and a secondary metabolic impact that predominantly maintains insulin sensitivity.

Key Words: Genetic animal models, Matrix mineralisation, Osteoblasts, Bone-fat interactions, non-collagenous proteins.

Introduction

Ecto-nucleotide pyrophosphatase/phosphodiesterase-1 (ENPP1 in humans, NPP1 in mice) is the founding member of the ENPP family – which comprises of seven structurally related isozymes (Mackenzie et al., 2012; Roberts, Zhu, Farquharson, & Macrae, 2019; Terkeltaub, 2006). Within bone, ENPP1 is highly expressed in the plasma membrane and mineral-depositing matrix vesicles (MV) of osteoblasts where its expression is over 30 times higher than in skeletal muscle (BioGPS, 2018; Roberts et al., 2019). ENPP1 is the principal generator of extracellular inorganic pyrophosphate (PP_i), a potent inhibitor of hydroxyapatite (HA) crystal formation in mineralisation-competent tissues (Mackenzie et al., 2012). Mice lacking NPP1 (*Enpp1*$^{-/-}$) have severe hypermineralisation defects, which are associated with abnormally low plasma PP_i levels (Huesa et al., 2014; Li et al., 2013; Mackenzie et al., 2012). We, and others, have previously reported the dramatic effects of global *Enpp1* ablation on soft tissue calcification and hyperostosis of vertebrae and joints, highlighting ENPP1 as a critical regulator of mineralisation through the production of PP_i (Anderson et al., 2005; Babij et al., 2009; Hajjawi et al., 2014; Harmey et al., 2004; Johnson et al., 2003; Johnson, Pritzker, Goding, & Terkeltaub, 2001).

Surprisingly we, and others, have indicated *Enpp1*$^{-/-}$ mice have reduced trabecular bone mass and cortical thickness of both the tibia and femur (Li et al., 2013; Mackenzie et al., 2012). This reduction may be a consequence of relatively low levels of endogenous NPP1 expression throughout the long bones when compared to flat bones such as calvaria (Anderson et al., 2005). For long bones, a complete ablation of NPP1 activity likely reduced extracellular PPi to abnormally low levels. Because of this, there is likely a reduced conversion of PPi to inorganic

phosphate (Pi) by tissue specific alkaline phosphatase (TNAP). This TNAP-specific breakdown of PPi to Pi is critical for normal mineral formation and this process is likely disrupted in *Enpp1*$^{-/-}$ mice.

Further to the action in the control of mineralisation, ENPP1 plays a recognised role in metabolic disease (Goldfine et al., 2008; Prudente, Morini, & Trischitta, 2009). Indeed, our studies challenging *Enpp1*$^{-/-}$ mice with chronic exposure to a high-fat diet (HFD) revealed that global *Enpp1* gene deletion promotes improved glucose homeostasis in the context of obesity-associated diabetes (Huesa et al., 2014). Whilst the tissue origin of the metabolically active ENPP1 is presently unknown, it is possible that ENPP1 function may be directly controlled through the actions of osteoblast-derived hormonally active osteocalcin. Osteocalcin is bioactive when in the under- or un-carboxylated state and is known to have insulin sensitising properties (Karsenty, Ferron, Karsenty, & Ferron, 2012; Karsenty & Olson, 2016)

In the present study, we hypothesised that osteoblast-specific NPP1 ablation results in reduced mineralisation of skeletal tissue and metabolic protection following chronic high-fat diet feeding. To test this we generated mice with osteoblast-specific deletion of *Enpp1* to determine their skeletal development and structure as well as metabolic changes associated with insulin sensitivity and glucose homeostasis.

Materials and Methods

Generation of osteoblast-specific *Enpp1* deficient mice

Floxed *Enpp1* mice (*fl/fl*) were generated by Cyagen Biosciences, (CA, USA). Osteocalcin-cre mice (*Ocn*-cre) were kindly donated by Thomas Clemens at John Hopkins Medicine, Baltimore, Maryland (Zhang et al., 2002). The commercially generated *fl/fl* mice were designed with the *loxP* sites around exon 9 (Supp. Fig. 1A) (Cyagen Biosciences, CA, USA). Mice were crossed to generate the osteoblast-specific conditional knockout mice (cKO) as well as appropriate *fl/fl* mice. PCR-based genotyping was performed on mouse DNA using a duplex PCR reaction for *Cre* (F:GCA TTA CCG GTC GAT GCA ACG AGT GAT GAG; R:GAG TGA ACG AAC CTG GTC GAA ATC AGT GCG) and *Fabpi200* (F:TGG ACA GGA CTG GAC CTC TGC TTT CCT AGA; R:TAG AGC TTT GCC ACA TCA CAG GTC ATT CAG) or *Enpp1* (F:GCTAATCATCAGGAGGTCAAG; R:CTGGTAGAATCCCGTCAATC). The specificity of the gene deletion was confirmed with western blot analysis of whole-bone tibial lysates (Supp. Fig 1B & 1C) with 85% efficiency of Cre recombinase activity. All mice were kept in polypropylene cages, with light/dark 12-hour cycles, at 21 ± 2°C. Mice for skeletal phenotyping (male and female mice) were fed *ad libitum* with control diet (6.2% fat; Harlan Laboratories, IN, USA) from 4- to 22-weeks of age. For metabolic phenotyping, only male mice were fed with a high-fat diet (HFD) (58% fat; Research Diets, Inc, New Brunswick, NJ, USA) or control diet (6.2% fat; Harlan Laboratories, IN, USA) from 4- to 16-weeks of age. For metabolic phenotyping, *ad libitum* food consumption and weight gain were monitored throughout the experiments. Roslin Institute's Animal Users Committee approved all experimental protocols and the animals were maintained in accordance with UK Home Office guidelines for the care and use of laboratory animals.

Glucose and insulin tolerance tests

16-week-old male mice were fasted for 4 hours and administered 2 mg of D-glucose (Sigma, Poole, UK) per g of body weight by oral gavage for glucose tolerance testing (GTT). For insulin tolerance testing (ITT), 16-week old male mice were fasted for 4 hours and administered 0.5 (control diet) or 0.75 (HFD) mU of insulin by intraperitoneal injection (Actrapid, NovoNordisk, Bagsvaerd, Denmark) per g of body weight. At 0, 15, 30, 60 and 120 minutes after insulin administration, blood glucose was measured with an Accu-Chek® Aviva glucose meter (Roche Diagnostics Ltd, Lewes, UK) and plasma insulin was measured by ELISA (ChrystalChem, Chicago, IL, USA). Mice were allowed to recover for up to one week before being culled. Tissues, including pancreas, kidney, quadriceps femoris, femora, humerus and tibiae as well as brown, subcutaneous, mesenteric and gonadal fat pads, were collected and fixed for at least 24 hours in 10% Neutral-buffered formalin (NBF) for histological assessment and gene expression analysis.

Plasma analysis

Immediately following euthanasia, blood was obtained from 6- and 16-week-old mice and plasma samples prepared. Blood was collected in eppendorfs coated with 2% EDTA on ice. After centrifugation (10 min, 1,000g, 4 ˚C), platelets were depleted from plasma by filtration (25 min, 2,200 g, 4 ˚C) through a Centrisart I 300,000 kD mass cutoff filter (Sartorius) and stored at -20 ˚C until further processing. Total, carboxylated (GLA), undercarboxylated (GLU13-OCN) and uncarboxylated (GLU) osteocalcin was measured as previously described (Ferron, Wei, Yoshizawa, Ducy, & Karsenty, 2010), as well as markers of bone formation (P1NP; AmsBio, Oxford) and resorption (CTx; AmsBio) and insulin, measured by ELISA

(ChrystalChem). The plasma PP_i concentration was determined as described previously (Robert S. Jansen et al., 2013).

Micro-computed tomography and mechanical testing

Tibiae and femora from 6-week-old male and female mice were dissected and were immediately fixed in 10% NBF for 24 hours and subsequently stored in 70% ethanol pending analysis. High-resolution scans with an isotropic voxel size of 4-5 µm were acquired with a micro-computed tomography system (µCT, 50 kV, 200uA Al filter, 0.4° rotation step, Skyscan 1172, Bruker microCT, Kontich, Belgium) as previously described (Hajjawi et al., 2014). Scans were reconstructed using NRecon software (Brukker microCT). For each bone, a 1 mm section of the metaphysis was analysed, using the base of the growth plate as a standard reference point. A 0.4 mm and 2.5 mm offset from the growth plate was used for trabecular and cortical bone, respectively. Data were analysed with CtAn software (Bruker microCT). For calculation of bone mineral density, an appropriate calibration of the Skyscan CT analyser was conducted using known density calcium hydroxyapatite phantoms scanned and reconstructed under identical conditions.

Tissue histology

Dissected soft tissues were fixed in 4% paraformaldehyde (PFA) or 10% NBF (pH 7.4), processed using standard protocols using a Leica Arcadia tissue processor, and embedded in paraffin wax. 4-8-µm sections (section thickness dependent on the stain used) were stained with haematoxylin and eosin (H&E) to assess tissue architecture and with Von Kossa or Alizarin Red-S to assess soft tissue calcification (Mackenzie et al., 2012). Liver sections were

stained with picrosirius red (with fast-green counter stain) to assess fibrosis (Henderson et al., 2013). Adipocyte diameter and number, and pancreatic β-cell islet number and size were quantified using ImageJ software as previously described (Huesa et al., 2014; Rueden et al., 2017). Long bones (femora and tibia) were fixed, decalcified in 10% ethylenediaminetetraacetic acid (EDTA) for 14 days at 4°C and embedded in wax. Subsequently, 4 µM sections were stained with H&E or toluidine blue. The femoral distal growth plate width was determined using Image J software (Rueden et al., 2017)

Primary calvarial osteoblast cell culture

Primary calvarial osteoblasts were isolated from the calvariae of 3- to 5-day-old mice as previously described (Huesa et al., 2014). Cells were seeded at a density of 100,000 cells/well in 6-well plates, in growth medium consisting of α-MEM (Invitrogen, Paisley, UK) supplemented with 10% FBS (Invitrogen) and 1% gentamicin (Invitrogen). Mineralisation was induced with the addition of 50µg/ml ascorbic acid and 5mM β-glycerophosphate as previously describe (Staines et al., 2017). In brief, cells were grown to confluence. Cells were maintained in a 5% CO_2 atmosphere at 37°C and the medium was changed every 2nd/3rd day. Cells were either processed for RNA extraction or fixed in 4% PFA and stained with 2% Alizarin Red S (pH 4.2) for 5 minutes at room temperature. Alizarin Red S-stained cultures were extracted with 10% cetylpyridinium chloride for 10 minutes and optical density was measured at 570 nm. Calcium deposition was also quantified based on a method previously described (Zhu, Mackenzie, Millan, Farquharson, & MacRae, 2013; Zhu et al., 2015). Briefly, cells were rinsed twice with phosphate-buffered saline (PBS) and decalcified with 0.6 M HCl at room temperature for 2 hours. Free calcium was determined colorimetrically by a stable interaction

with phenolsulphonethalein, using a commercially available kit (Randox Laboratories Ltd., County Antrim, UK).

Western blotting

The bone marrow of bones (humeri) was removed by centrifugation, and bones were homogenised in RIPA buffer (Sigma) with protease inhibitor cocktail (Sigma) using an IKA homogeniser (Sigma, UK). Western blotting was conducted with specific antibodies against ENPP1 (Pierce, Waltham, MA, USA) and β-actin (Abcam) and performed as previously described (Zhu et al., 2013; Zhu, Mackenzie, Millán, Farquharson, & MacRae, 2011) and visualised using the enhanced chemiluminescence (ECL) western blotting detection system (GE Healthcare, Chalfont St Giles, UK).

RNA extraction and qPCR

RNA was isolated from bone (bone marrow removed), muscle and fat tissues using Qiazol (Qiagen, Valencia, CA, USA) following standard protocol procedures. RNA from all other tissues and cell cultures were extracted with the RNeasy Qiagen kit following the manufacturers' instructions (Qiagen). RNA was quantified and reverse transcribed as previously described (Zhu et al., 2011). All genes were analysed with the SYBR green detection method (Roche) using the Stratagene Mx3000P real-time QPCR system (Agilent Technologies, Santa Clara, CA, USA). All gene expression data were normalised against *β-actin*. All primers (*Tnap, Runx2, phospho1 and Ank*) were obtained from Qiagen, Sigma and Primer Design (Primer Design, Southampton, UK).

Statistics

Data are expressed as the mean ± SEM of at least three replicates per experiment. Standard comparisons between mice genotypes were analysed by unpaired Student's *t*-test. Comparisons between genotype and diet were analysed with two-way ANOVA. Time-course experiments were analysed with a repeated-measures two-way ANOVA. Analysis was carried out using Minitab 16 (Minitab Ltd, Coventry, UK). A p-value of < 0.05 was considered to be significant; p-values of <0.05, <0.01 and <0.001 were noted as *, ** and ***, respectively.

Results

Enpp1 deletion in osteoblasts results in increased trabecular bone mass in female mice

Comprehensive high-resolution μ-CT scanning revealed gender-dependent effects on tibial and femoral trabecular structural parameters, and less so in cortical bone. Examination of the mid-diaphyseal cortical bone of femora from 6-week old female cKO mice showed increased femoral bone volume/total volume (17.50% vs 11.67%; $p<0.01$), endosteal diameter (1.95 mm vs. 1.67 mm; $p<0.001$) and open porosity (2.46% vs. 2.04%; $p<0.05$) compared to femora from female *fl/fl* mice (Table 1). 6-week old female cKO also exhibit increased tibia endosteal diameter (1.48 mm vs. 1.29 mm; $p<0.001$) compared to femora from female *fl/fl* mice (Table 1).

Male 6-week old cKO mice demonstrate reduced cortical thickness 0.109 mm vs. 0.117 mm; $p<0.05$) in the mid-diaphyseal femoral bone, and increased tibial periosteal diameter (1.817 mm vs. 1.660 mm; $p<0.05$) compared to male *fl/fl* mice (Table 1). No differences in long bone trabecular parameters were observed for male mice (Table 2). In addition, female cKO mice showed decreased trabecular pattern factor (15.29 vs. 23.33; $p<0.01$, Table 2; Supp. Fig 1D & 1E) in the trabecular compartment of the femur. The structure model index (SMI), which quantifies the architecture of a 3D structure in terms of amounts of plates and rods composing the structure (Hildebrand & Ruegsegger, 1997), was also significantly lower in femora from female cKO mice (1.39 vs. 1.66; $p<0.01$, Table 2) compared to *fl/fl* mice. This indicates that the trabeculae in cKO mice appear to be more 'plate-like' and more connected. Comparable changes were also observed in the tibia of cKO female mice. Interestingly, no differences in the bone-resorption marker CTx (Supp. Fig. 1F) or the bone-formation marker P1NP (Supp. Fig. 1F) were observed.

Mice with osteoblast-specific ablation of *Enpp1 show* physiological plasma levels of the mineralisation inhibitor PPi

We next addressed whether the cKO mice displayed depressed levels of PP_i, resembling that previously reported for *Enpp1*$^{-/-}$ mice (Terkeltaub, 2006). No notable differences in PP_i levels in male or female mice (Supp. Fig. 1H) were observed. Subsequent alizarin red staining of metabolically - related soft tissues (e.g. pancreas) mineralisation-related soft tissues (e.g. whisker follicle, aorta) and viscera tissues reveals an absence of pathological calcification (Supp. Fig. 2 A-J) in cKO mice when compared to *fl/fl* mice. Furthermore, absence of pathological calcification was also observed in femorotibial joint (Supp. Fig. 2 K-L).

Enpp1* deficient osteoblasts exhibit an enhanced ability to mineralise a matrix *in vitro

To assess whether NPP1 plays a key role in osteoblast-mediated mineralisation, we analysed calcium deposition in 28-day cultured cKO osteoblasts, in comparison to *fl/fl* cells. Qualitative (Fig. 1A) and quantitative (Fig. 1B, C) analyses of calcium deposition indicated an enhanced ability of cKO osteoblasts to calcify their matrix. We also examined the mRNA expression of key osteogenic and mineralisation associated genes in cKO osteoblasts. *Alpl, Runx2 and Phospho1* were all significantly increased in cKO osteoblasts compared to *fl/fl* cells following culture until cellular monolayer confluence was reached (termed day 0) ($P<0.05$) (Fig. 1D). No differences in the mRNA expression levels of the PP_i transporter *Ank* were noted (Fig. 1D).

Male mice with osteoblast-specific ablation of *Enpp1* show normal glucose tolerance and an elevated bioactive osteocalcin levels

We next tested whether the osteoblast-specific deletion of *Enpp1* also translates into changes in whole-body glucose metabolism in male mice. 16-week old male cKO and *fl/fl* male mice fed the control-diet showed similar glucose and insulin tolerance (Supp. Fig. 3A-D). The size and number of pancreatic islets in control-diet fed cKO and *fl/fl* male mice were similar (Supp. Fig 3A, B). Additionally, there were no differences in fat pad mass (Supp. Fig. 4C) or white fat (subcutaneous, gonadal or mesenteric) morphology (Supp. Fig. 4D, E). Furthermore, no changes in mRNA expression levels of key genes for glucose transport (*Slc2a1*, *Slc2a4*, *Slc2a10*, *Slc2a12*) in gonadal fat were found (data not shown).

A significant increase in left and right *quadratus femoris* muscle mass from the control-diet fed cKO mice was observed when compared with *fl/fl* mice (left: 8.45 mg vs. 7.46 mg; $p<0.05$, right: 8.48 mg vs 7.38 mg, $P<0.05$) (Fig. 2A).

We recently published novel findings revealing that global *Enpp1*$^{-/-}$ mice have increased levels of the insulin-sensitising bone-derived hormone osteocalcin (Huesa et al., 2014). The present study established that this observation may be specific to the actions of NPP1 in osetoblasts, with cKO mice also exhibiting significantly increased concentrations of undercarboxylated (GLU13) and osteocalcin (22.87 ng/ml vs. 11.74 ng/ml; $p<0.05$) (Fig. 2B) (Ferron et al., 2010). Total osteocalcin levels were comparable to *fl/fl* mice (Fig. 2C).

Male mice with osteoblast-specific ablation of *Enpp1* exhibit insulin resistance in response to chronic HFD challenge

We next investigated the effect of chronic high fat diet feeding on whole body glucose metabolism in 16-week old male cKO mice. Following chronic HFD-challenge (12 weeks), no significant differences were observed between genotypes in body weight gain (Fig. 3A), pancreatic islet morphology (Fig. 3B, C) or white fat mass (Fig. 3D) of male mice. However, cKO male mice showed a significant increase in brown fat mass (22.2%; $p<0.05$; Fig. 3D). Furthermore, the gonadal fat depot of the cKO male mice showed decreased average number of adipocytes per micrograph (85.19 vs. 283.19, $p<0.001$) (Fig. 3E) and increased average adipocyte area (6215 μm^2 vs. 3051.28 μm^2, $p<0.01$) (Fig. 3F) compared to *fl/fl* male mice.

Impaired glucose tolerance ($p<0.05$; Fig. 4A, D) and reduced insulin sensitivity was observed in HFD challenged cKO male mice ($p<0.05$; Fig. 4B, D). However, no significant difference was observed between genotypes in glucose-stimulated insulin secretion (GSIS) (Fig. 4C, D), indicative of relative preservation of normal β-cell function and peripheral insulin resistance in the male mice.

Discussion

The mineralisation process depends on a regulated balance of various protein inducers and inhibitors. Indeed the application of mutant mouse models lacking NPP1 has highlighted the crucial role of NPP1 in regulating bone mineralisation. However, these mice surprisingly show an osteopenic phenotype, despite the depressed levels of the circulating mineralisation inhibitor PP_i (Mackenzie et al., 2012). Our present study reveals for the first time the precise role of osteoblastic NPP1 bone formation; with a specific ablation of NPP1 from osteoblasts increasing bone mass evidenced through bone volume fraction (BV/TV) parameters. Indeed, a notable increase in bone volume/total volume was observed in female mice (Table 2). The lack of bone changes in the male compared to female mice may be underpinned by the different signalling pathways activated by the androgen and oestrogen receptors within bone and warrants further investigation.

Calvarial osteoblasts lacking NPP1 showed increased mineralisation potential *in vitro*, consistent with increased markers of osteogenic differentiation and mineralisation. These novel data suggest that the local generation of PP_i from nucleotide precursors by NPP1 within the bone micro-environment directly regulates the ratio of P_i to PP_i, controlling the deposition of bone mineral. This ratio may be further modified by the upregulated *Alpl* expression observed in cKO osteoblasts, which may accelerate PP_i degradation and the simultaneous generation of P_i, thus promoting mineralisation. Indeed ablating both NPP1 and TNAP function in mice has previously highlighted site-specific effects of NPP1, with normalisation of the degree of mineralisation seen in the joints, vertebrae and soft tissues, yet hypomineralisation of the long bones remaining (Millán, 2013). Relatively low levels of endogenous NPP1 expression in long bones compared to other tissues, reducing extracellular PP_i to abnormally low levels was proposed to underpin this phenotype.

This study reveals that osteoblast specific NPP1 ablation is not sufficient to replicate the severe hypermineralisation of the connective tissues, including significant arterial calcification, observed in adult *Enpp1*$^{-/-}$ mice (Mackenzie et al., 2012). Additionally, these cKO mice do not show vertebrae hyperostosis or excessive bone production in the femorotibial joint, in contrast to *Enpp1*$^{-/-}$ mice. Together these results suggest that the circulatory PP_i generated from liver-derived NPP1 may be exerting crucial systemic protective effects against ectopic mineralisation. Thus, the prevailing mechanistic hypothesis suggests that ATP-binding cassette C6 (ABCC6) mediates ATP release within the liver (R. S. Jansen et al., 2014). This ATP is subsequently hydrolysed by hepatic ENPP1 to PP_i, which acts as an endocrine inhibitor of calcification at distant target sites. Indeed, ectopic mineralisation and reduced circulating PP_i levels are observed in *Abcc6* deficient mice. Interestingly, *Abcc6*$^{-/-}$ which constitutively express human ENPP1 show increased plasma PP_i levels with small mineralisation foci within connective tissues. This indicates an alternative mechanism, independent of PP_i, by which ABCC6 prevents ectopic mineralisation (Zhao, Kingman, Sundberg, Uitto, & Li, 2017). This mechanism may work in tandem with CD73, an ecto-5'-nucleotidase that degrades AMP to adenosine and P_i (St Hilaire et al., 2011), to maintain low TNAP levels and prevent pathological mineralisation (Ziegler et al., 2017). Further investigations examining the tissue specific contribution of NPP1 from liver will be key to elucidating the precise role of NPP1 in this multi-faceted pathway.

NPP1 negatively modulates insulin receptor signalling and has been proposed as a pathogenic factor predisposing to insulin resistance (Goldfine et al., 2008; Prudente et al., 2009). Indeed our laboratory has recently provided key evidence highlighting that NPP1 ablation protects against insulin resistance, obesity and diabetes (Huesa et al., 2014). Following the recent

emergence of bone as an endocrine regulator, and given the fundamental importance of NPP1 in bone mineralisation, it is essential to elucidate the contribution of osteoblastic NPP1 to the regulation of glucose metabolism. Intriguingly, we show here that osteoblast-specific NPP1 deficiency drives an unexpected worsening of insulin sensitivity relative to *fl/fl* mice chronically exposed to a high-fat diet, despite elevated levels of the insulin-sensitising form of osteocalcin.

Furthermore, these mice demonstrate white (gonadal, mesenteric and sub-cutaneous depots) adipose tissue hypertrophy which is reported in the literature to be associated with metabolic impairment including insulin resistance (Kim et al., 2014). The cKO mice also present with a notable increase in brown adipose tissue mass of 22%. This is likely due to the mild thermogenic stress of room-temperature housing whereby the mice undergo alterations in non-shivering thermogenesis, which over time increases brown adipose tissue mass and activity (Feldmann, Golozoubova, Cannon, & Nedergaard, 2009; Lim et al., 2012; Nedergaard & Cannon, 2010; Xue et al., 2009). However, no significant differences in the mRNA levels of genes like solute carrier family 2 member 1 and 4 (*Slc2a1*, *slc2a4*), diacylglycerol O-acyltransferase 1 and 2 (*Dgat1* and *Dgat2*), uncoupling protein 1 and 2 *(Ucp1, Ucp2) and* lipoprotein lipase *(Lpl)* associated with thermogenic functionality were observed (Supp. Fig. 5). The links between brown adipose tissue and bone are established, including positive correlation of brown adipose tissue volume and bone mineral density and bone cross sectional area (Bredella et al., 2012; Bredella, Gill, Rosen, Klibanski, & Torriani, 2014; P. Lee et al., 2013). Our data suggests that osteoblast-specific NPP1 may be important in regulating bone and brown fat tissue homeostasis and subsequent brown adipose tissue activity. Additionally, the cKO mice present with increased *quadriceps femoris* muscle, yet do not

present with metabolic protection. As such, it is likely that this *quadriceps femoris* muscle increase is not associated with the protective cardiometabolic effects observed in chronic caloric excess (e.g. obesity) as reported for increased appendicular skeletal mass in other mouse studies (Lee et al., 2019). These data suggest that the protection against diabetes reported in *Enpp1*$^{-/-}$ mice is likely due to the actions of non-skeletal NPP1 and indicate that NPP1 inhibition at one of its major sites of expression is metabolically detrimental. Interestingly, a differential sex-related sensitivity has been reported in obesity and insulin resistance-related cardio-metabolic diseases, with a lower incidence of these pathologies being observed in young female mice when compared to age-matched males. Future investigations assessing insulin metabolism in female cKO mice would advance our understanding of the mechanisms underlying these sex-related changes in the susceptibility to diabetes and obesity.

Hormonally active osteocalcin (under- and un-carboxylated forms) acts to increase insulin secretion through β-cell proliferation and augments peripheral insulin sensitivity and energy expenditure (Ferron et al., 2010; Fulzele et al., 2010). We recently demonstrated that global *Enpp1*$^{-/-}$ mice have elevated levels of active osteocalcin and remain insulin sensitive following chronic high-fat diet feeding (Huesa et al., 2014). Here we show that the insulin-resistant cKO mice also similarly exhibit increased concentrations of undercarboxylated and bioactive osteocalcin. This suggests that osteocalcin regulation is a specific consequence of NPP1 in bone, with bone ENPP1 deficiency driving the increased plasma osteocalcin levels. These data support previous reports highlighting an osteocalcin-independent influence of osteoblasts on energy metabolism (Yoshikawa et al., 2011).

In conclusion, our data adds to the body of evidence supporting a role for ENPP1 in metabolic dysfunction. We demonstrate that osteoblast-specific ablation of NPP1 in mice alters osteocalcin carboxylation status whilst offering reduced protection against insulin resistance. Furthermore, future work assessing a wider range of bone phenotypes, including osteoclast function and comparison of appendicular to axial bones in these mice would be highly informative. A fuller understanding of the tissue-specific actions of ENPP1 is undoubtedly required to inform the development of new therapeutic strategies for treating diabetes.

References

Anderson, H. C., Harmey, D., Camacho, N. P., Garimella, R., Sipe, J. B., Tague, S., . . . Millan, J. L. (2005). Sustained osteomalacia of long bones despite major improvement in other hypophosphatasia-related mineral deficits in tissue nonspecific alkaline phosphatase/nucleotide pyrophosphatase phosphodiesterase 1 double-deficient mice. *Am J Pathol, 166*(6), 1711-1720. doi:10.1016/s0002-9440(10)62481-9

Babij, P., Roudier, M., Graves, T., Han, C. Y., Chhoa, M., Li, C. M., . . . Carlson, G. (2009). New variants in the Enpp1 and Ptpn6 genes cause low BMD, crystal-related arthropathy, and vascular calcification. *J Bone Miner Res, 24*(9), 1552-1564. doi:10.1359/jbmr.090417

BioGPS. (2018). Retrieved from http://biogps.org/#goto=genereport&id=5167

Bredella, M. A., Fazeli, P. K., Freedman, L. M., Calder, G., Lee, H., Rosen, C. J., & Klibanski, A. (2012). Young women with cold-activated brown adipose tissue have higher bone mineral density and lower Pref-1 than women without brown adipose tissue: a study in women with anorexia nervosa, women recovered from anorexia nervosa, and normal-weight women. *J Clin Endocrinol Metab, 97*(4), E584-590. doi:10.1210/jc.2011-2246

Bredella, M. A., Gill, C. M., Rosen, C. J., Klibanski, A., & Torriani, M. (2014). Positive effects of brown adipose tissue on femoral bone structure. *Bone, 58*, 55-58. doi:10.1016/j.bone.2013.10.007

Feldmann, H. M., Golozoubova, V., Cannon, B., & Nedergaard, J. (2009). UCP1 Ablation Induces Obesity and Abolishes Diet-Induced Thermogenesis in Mice Exempt from Thermal Stress by Living at Thermoneutrality. *Cell Metabolism, 9*(2), 203-209. doi:https://doi.org/10.1016/j.cmet.2008.12.014

Ferron, M., Wei, J., Yoshizawa, T., Ducy, P., & Karsenty, G. (2010). An ELISA-based method to quantify osteocalcin carboxylation in mice. *Biochemical and biophysical research communications, 397*(4), 691-696. doi:10.1016/j.bbrc.2010.06.008

Fulzele, K., Riddle, R. C., DiGirolamo, D. J., Cao, X., Wan, C., Chen, D., . . . Clemens, T. L. (2010). Insulin receptor signaling in osteoblasts regulates postnatal bone acquisition and body composition. *Cell, 142*(2), 309-319. doi:10.1016/j.cell.2010.06.002

Goldfine, I. D., Maddux, B. A., Youngren, J. F., Reaven, G., Accili, D., Trischitta, V., . . . Frittitta, L. (2008). The role of membrane glycoprotein plasma cell antigen 1/ectonucleotide pyrophosphatase phosphodiesterase 1 in the pathogenesis of insulin resistance and related abnormalities. *Endocr Rev, 29*(1), 62-75. doi:10.1210/er.2007-0004

Hajjawi, M., Macrae, V., Huesa, C., Boyde, A., Luis Millán, J., Arnett, T., & Orriss, I. (2014). *Mineralisation of collagen rich soft tissues and osteocyte lacunae in Enpp1(-/-) mice* (Vol. 69).

Harmey, D., Hessle, L., Narisawa, S., Johnson, K. A., Terkeltaub, R., & Millán, J. L. (2004). Concerted Regulation of Inorganic Pyrophosphate and Osteopontin by Akp2, Enpp1, and Ank: An Integrated Model of the Pathogenesis of Mineralization Disorders. *The American Journal of Pathology, 164*(4), 1199-1209. doi:https://doi.org/10.1016/S0002-9440(10)63208-7

Henderson, N. C., Arnold, T. D., Katamura, Y., Giacomini, M. M., Rodriguez, J. D., McCarty, J. H., . . . Sheppard, D. (2013). Targeting of αv integrin identifies a core molecular pathway that regulates fibrosis in several organs. *Nature medicine, 19*(12), 1617-1624. doi:10.1038/nm.3282

Hildebrand, T., & Ruegsegger, P. (1997). Quantification of Bone Microarchitecture with the Structure Model Index. *Comput Methods Biomech Biomed Engin, 1*(1), 15-23. doi:10.1080/01495739708936692

Huesa, C., Zhu, D., Glover, J. D., Ferron, M., Karsenty, G., Milne, E. M., . . . MacRae, V. E. (2014). Deficiency of the bone mineralization inhibitor NPP1 protects mice against obesity and diabetes. *Disease models & mechanisms, 7*(12), 1341-1350. doi:10.1242/dmm.017905

Jansen, R. S., Duijst, S., Mahakena, S., Sommer, D., Szeri, F., Varadi, A., . . . van de Wetering, K. (2014). ABCC6-mediated ATP secretion by the liver is the main source of the mineralization

inhibitor inorganic pyrophosphate in the systemic circulation-brief report. *Arterioscler Thromb Vasc Biol, 34*(9), 1985-1989. doi:10.1161/ATVBAHA.114.304017

Jansen, R. S., Küçükosmanoğlu, A., de Haas, M., Sapthu, S., Otero, J. A., Hegman, I. E. M., . . . van de Wetering, K. (2013). ABCC6 prevents ectopic mineralization seen in pseudoxanthoma elasticum by inducing cellular nucleotide release. *Proceedings of the National Academy of Sciences, 110*(50), 20206. doi:10.1073/pnas.1319582110

Johnson, K., Goding, J., Van Etten, D., Sali, A., Hu, S. I., Farley, D., . . . Terkeltaub, R. (2003). Linked deficiencies in extracellular PP(i) and osteopontin mediate pathologic calcification associated with defective PC-1 and ANK expression. *J Bone Miner Res, 18*(6), 994-1004. doi:10.1359/jbmr.2003.18.6.994

Johnson, K., Pritzker, K., Goding, J., & Terkeltaub, R. (2001). The nucleoside triphosphate pyrophosphohydrolase isozyme PC-1 directly promotes cartilage calcification through chondrocyte apoptosis and increased calcium precipitation by mineralizing vesicles. *The Journal of Rheumatology, 28*(12), 2681.

Karsenty, G., Ferron, M., Karsenty, G., & Ferron, M. (2012). The contribution of bone to whole-organism physiology. *Nature, 481*, 314-320.

Karsenty, G., & Olson, E. N. (2016). Bone and Muscle Endocrine Functions: Unexpected Paradigms of Inter-organ Communication. *Cell, 164*(6), 1248-1256. doi:10.1016/j.cell.2016.02.043

Kim, Soo M., Lun, M., Wang, M., Senyo, Samuel E., Guillermier, C., Patwari, P., & Steinhauser, Matthew L. (2014). Loss of White Adipose Hyperplastic Potential Is Associated with Enhanced Susceptibility to Insulin Resistance. *Cell Metabolism, 20*(6), 1049-1058. doi:https://doi.org/10.1016/j.cmet.2014.10.010

Lee, Kim, E. H., Bae, S. J., Choe, J., Jung, C. H., Lee, W. J., & Kim, H. K. (2019). Protective role of skeletal muscle mass against progression from metabolically healthy to unhealthy phenotype. *Clin Endocrinol (Oxf), 90*(1), 102-113. doi:10.1111/cen.13874

Lee, P., Brychta, R. J., Collins, M. T., Linderman, J., Smith, S., Herscovitch, P., . . . Celi, F. S. (2013). Cold-activated brown adipose tissue is an independent predictor of higher bone mineral density in women. *Osteoporos Int, 24*(4), 1513-1518. doi:10.1007/s00198-012-2110-y

Li, Q., Guo, H., Chou, D. W., Berndt, A., Sundberg, J. P., & Uitto, J. (2013). Mutant Enpp1asj mice as a model for generalized arterial calcification of infancy. *Disease models & mechanisms, 6*(5), 1227-1235. doi:10.1242/dmm.012765

Lim, S., Honek, J., Xue, Y., Seki, T., Cao, Z., Andersson, P., . . . Cao, Y. (2012). Cold-induced activation of brown adipose tissue and adipose angiogenesis in mice. *Nature Protocols, 7*(3), 606-615. doi:10.1038/nprot.2012.013

Mackenzie, N. C. W., Zhu, D., Milne, E. M., van 't Hof, R., Martin, A., Quarles, D. L., . . . MacRae, V. E. (2012). Altered Bone Development and an Increase in FGF-23 Expression in Enpp1−/− Mice. *PLOS ONE, 7*(2), e32177. doi:10.1371/journal.pone.0032177

Millán, J. L. (2013). The role of phosphatases in the initiation of skeletal mineralization. *Calcified tissue international, 93*(4), 299-306. doi:10.1007/s00223-012-9672-8

Nedergaard, J., & Cannon, B. (2010). The Changed Metabolic World with Human Brown Adipose Tissue: Therapeutic Visions. *Cell Metabolism, 11*(4), 268-272. doi:https://doi.org/10.1016/j.cmet.2010.03.007

Prudente, S., Morini, E., & Trischitta, V. (2009). Insulin signaling regulating genes: effect on T2DM and cardiovascular risk. *Nat Rev Endocrinol, 5*(12), 682-693. doi:10.1038/nrendo.2009.215

Roberts, F., Zhu, D., Farquharson, C., & Macrae, V. (2019). *ENPP1 in the Regulation of Mineralization and Beyond*.

Rueden, C. T., Schindelin, J., Hiner, M. C., DeZonia, B. E., Walter, A. E., Arena, E. T., & Eliceiri, K. W. (2017). ImageJ2: ImageJ for the next generation of scientific image data. *BMC Bioinformatics, 18*(1), 529. doi:10.1186/s12859-017-1934-z

St Hilaire, C., Ziegler, S. G., Markello, T. C., Brusco, A., Groden, C., Gill, F., . . . Boehm, M. (2011). NT5E mutations and arterial calcifications. *N Engl J Med, 364*(5), 432-442. doi:10.1056/NEJMoa0912923

Staines, K. A., Javaheri, B., Hohenstein, P., Fleming, R., Ikpegbu, E., Unger, E., . . . Farquharson, C. (2017). Hypomorphic conditional deletion of E11/Podoplanin reveals a role in osteocyte dendrite elongation. *Journal of cellular physiology, 232*(11), 3006-3019. doi:10.1002/jcp.25999

Terkeltaub, R. (2006). Physiologic and pathologic functions of the NPP nucleotide pyrophosphatase/phosphodiesterase family focusing on NPP1 in calcification. *Purinergic signalling, 2*(2), 371-377. doi:10.1007/s11302-005-5304-3

Xue, Y., Petrovic, N., Cao, R., Larsson, O., Lim, S., Chen, S., . . . Cao, Y. (2009). Hypoxia-Independent Angiogenesis in Adipose Tissues during Cold Acclimation. *Cell Metabolism, 9*(1), 99-109. doi:https://doi.org/10.1016/j.cmet.2008.11.009

Yoshikawa, Y., Kode, A., Xu, L., Mosialou, I., Silva, B. C., Ferron, M., . . . Kousteni, S. (2011). Genetic evidence points to an osteocalcin-independent influence of osteoblasts on energy metabolism. *J Bone Miner Res, 26*(9), 2012-2025. doi:10.1002/jbmr.417

Zhang, M., Xuan, S., Bouxsein, M. L., von Stechow, D., Akeno, N., Faugere, M. C., . . . Clemens, T. L. (2002). Osteoblast-specific knockout of the insulin-like growth factor (IGF) receptor gene reveals an essential role of IGF signaling in bone matrix mineralization. *J Biol Chem, 277*(46), 44005-44012. doi:10.1074/jbc.M208265200

Zhao, J., Kingman, J., Sundberg, J. P., Uitto, J., & Li, Q. (2017). Plasma PPi Deficiency Is the Major, but Not the Exclusive, Cause of Ectopic Mineralization in an Abcc6(-/-) Mouse Model of PXE. *J Invest Dermatol, 137*(11), 2336-2343. doi:10.1016/j.jid.2017.06.006

Zhu, D., Mackenzie, N. C. W., Millan, J. L., Farquharson, C., & MacRae, V. E. (2013). A protective role for FGF-23 in local defence against disrupted arterial wall integrity? *Molecular and cellular endocrinology, 372*(1-2), 1-11. doi:10.1016/j.mce.2013.03.008

Zhu, D., Mackenzie, N. C. W., Millán, J. L., Farquharson, C., & MacRae, V. E. (2011). The Appearance and Modulation of Osteocyte Marker Expression during Calcification of Vascular Smooth Muscle Cells. *PLOS ONE, 6*(5), e19595. doi:10.1371/journal.pone.0019595

Zhu, D., Mackenzie, N. C. W., Shanahan, C. M., Shroff, R. C., Farquharson, C., & MacRae, V. E. (2015). BMP-9 regulates the osteoblastic differentiation and calcification of vascular smooth muscle cells through an ALK1 mediated pathway. *Journal of cellular and molecular medicine, 19*(1), 165-174. doi:10.1111/jcmm.12373

Ziegler, S. G., Ferreira, C. R., MacFarlane, E. G., Riddle, R. C., Tomlinson, R. E., Chew, E. Y., . . . Dietz, H. C. (2017). Ectopic calcification in pseudoxanthoma elasticum responds to inhibition of tissue-nonspecific alkaline phosphatase. *Sci Transl Med, 9*(393). doi:10.1126/scitranslmed.aal1669

Tables

Table 1. Micro-CT analysis of the femur and tibia cortical bone from 6-week old male and female cKO and *fl/fl* mice. Data presented as the mean ± S.E.M. (n≥4). Significance is denoted by P<0.05, **P<0.01, ***P<0.001.

Bone	Gender	Genotype	Peri. Di (mm)	Endo. Di (mm)	BV (mm^3)	Tb. Th (mm)	Po(op) (%)
Femur	Male	*fl/fl*	2.144 (0.06)	1.773 (0.06)	0.800 (0.05)	0.117 (0.00)	2.059 (0.30)
		cKO	2.147 (0.04)	1.783 (0.06)	0.815 (0.02)	0.109 (0.00)*	2.828 (0.19)
	Female	*fl/fl*	1.97 (0.03)	1.67 (0.03)	0.565 (0.03)	0.106 (0.02)	2.04 (0.09)
		cKO	2.25 (0.03)	1.95 (0.03)***	0.64 (0.04)	0.100 (0.03)	2.46 (0.14)*
Tibia	Male	*fl/fl*	1.66 (0.05)*	1.277 (0.07)	0.857 (0.04)	0.101 (0.01)	3.467 (0.50)
		cKO	1.817 (0.02)	1.357 (0.03)	0.859 (0.02)	0.09 (0.00)	4.128 (0.29)
	Female	*fl/fl*	1.57 (0.13)	1.29 (0.02)	0.624 (0.02)	0.09 (0.02)	3.35 (0.28)
		cKO	1.89 (0.04)*	1.48 (0.03)***	0.68 (0.03)	0.08 (0.03)	3.53 (0.16)

Table 2. Micro-CT analysis of the femur and tibia trabecular parameters of 6-week old male and female cKO and *fl/fl* mice. Data presented as the mean ± S.E.M. (n≥5). Significance is denoted by *P<0.05, **P<0.01, ***P<0.001.

Bone	Gender	Genotype	BV/TV %	BMD (g/cm^3)	Tb. Pf	Tb. Th (µm)	Tb. No	Tb. Sp (mm)	SMI
Femur	Male	*fl/fl*	22.40 (1.98)	0.31 (0.02)	7.24 (3.04)	41.1 (0.00)	5.24 (0.34)	0.14 (0.11)	1.05 (0.55)
		cKO	26.96 (5.88)	0.30 (0.03)	4.15 (2.80)	44.38 (0.00)	6.023 (0.26)	0.13 (0.03)	0.928 (0.31)
	Female	*fl/fl*	11.99 (0.65)	0.32 (0.01)	23.22 (1.48)	36.37 (0.00)	3.29 (0.13)	0.19 (0.00)	1.668 (0.05)
		cKO	17.50*** (0.58)	0.36 (0.02)	15.29** (1.42)	38.06 (0.00)	4.61*** (0.15)	0.18 (0.00)	1.39 ** (0.05)
Tibia	Male	*fl/fl*	16.60 (1.55)	0.246 (0.01)	22.43 (2.50)	39.80 (0.00)	4.12 (0.26)	0.14 (0.01)	1.77 (0.09)
		cKO	16.68 (0.94)	0.26 (0.02)	21.59 (1.93)	40.15 (0.00)	4.12 (0.15)	0.15 (0.00)	1.71 (0.05)
	Female	*fl/fl*	7.675 (0.57)	0.16 (0.01)*	34.79 (2.70)	34.18 (0.09)	2.24 (0.16)	0.22 (0.01)	2.03 (0.09)
		cKO	10.92** (0.72)	0.198 (0.01)	29.76 (3.38)	33.62 (0.00)	3.23*** (0.12)	0.18*** (0.01)	1.85 (0.06)

Figure legends

Figure 1. The matrix of *Enpp1* deficient calvariae osteoblasts show a hypermineralized phenotype *in vitro*. (A) Representative image of alizarin red stained primary osteoblast cells, (B) Quantification of alizarin red stain, (C) Quantification of total calcium and (D) Relative mRNA expression of osteogenic and mineralization markers including *Tnap, Runx2, Phospho1 and Ank at day 0* . Data are presented as the mean ± S.E.M (n=6). Significance is denoted by *P<0.05, **P<0.01, ***P<0.001.

Figure 2. cKO mice display an altered *quadriceps femoris* mass and osteocalcin levels. (A) Muscle mass of male cKO and *fl/fl* mice at 16-weeks of age (n=6). (B) Undercarboxylated OCN levels and (C) total OCN levels in 16-week old male *fl/fl* and cKO mice (n=6). Data are presented as the mean ± S.E.M. Significance is denoted by *P<0.05.

Figure 3. Assessment of pancreatic and fat tissue morphology in cKO and *fl/fl* male mice following a chronic HFD challenge. (A) Weekly weight gain of HFD challenged cKO and *fl/fl* mice (n≥7). (B) Pancreatic islet area and (C) Islet number (n≥4) (D) Average mass of brown (B), sub-cutaneous (SC), gonadal (G) and mesenteric (Mes) fat (n≥4). The average (E) number and (F) area of adipocytes in SC, G and Mes fat (n≥4) of HFD challenged cKO and *fl/fl* mice at 16-weeks of age. Data are presented as the mean ± S.E.M. Significance is denoted by *P<0.05, **P<0.01, ***P<0.001.

Figure 4. cKO mice show increased insulin resistance in response to a chronic HFD challenge. (A) Insulin tolerance test (B) Glucose tolerance test and (C) Glucose stimulated insulin secretion (GSIS). (D) Metabolic tests analysed as area under the curve.

Mice were reared under high-fat dietary conditions and were 16-weeks of age. Data are presented as the mean ± S.E.M (n≥6). Significance is denoted by *P<0.05, **P<0.01, ***P<0.001.

Supplementary Figure 1. cKO mice show unaltered plasma markers of bone resorption and formation and unaltered plasma pyrophosphate. (A) Schematic showing the generation of cKO mice and (B) western blot of NPP1 in humeri samples of *fl/fl* and cKO mice (n=3) & (C) quantification of NPP1 was obtained with densitometry analysis, and normalized with β-actin. (n=3). 3D reconstruction of the (D) *fl/fl* and (E) cKO female trabecular bone scanned using micro-CT. (F) CTx and (G) P1NP levels in 6-week old male and female cKO and *fl/fl* mice (n=6). (H) Plasma PP_i concentrations from male and female cKO and *fl/fl* mice (n=6). Data are presented as the mean ± S.E.M. Significance is denoted by *P<0.05, **P<0.01, ***P<0.001.

Supplementary Figure 2. Alizarin red and H&E staining of tissues from cKO and *fl/fl* mice.

Alizarin red staining (A, B) Kidney (C, D) Liver, (E, F) Heart, (G, H) Aorta (I, J) Vibrissae and (K, L) H&E staining of Femorotibial joint (M) positive control, Scale bar = 40 µm.

Supplementary Figure 3. cKO mice fed control diet show normal glucose and insulin metabolism. (A) Glucose tolerance test, (B) Insulin tolerance test and (C) Glucose stimulated

insulin secretion (GSIS). (D) Metabolic tests analysed as area under the curve. cKO and *fl/fl* mice were reared under control dietary conditions and were 16 weeks of age. Data are presented as the mean ± S.E.M (n≥6). Significance is denoted by *P<0.05, **P<0.01, ***P<0.001.

Supplementary Figure 4. Histological assessment of pancreatic and fat tissues from cKO and *fl/fl* mice. (A) Pancreatic islet area and (B) number (n≥4). (C) Average mass of brown (B), sub-cutaneous (SC), gonadal (G) and mesenteric (Mes) fat (n≥9). The average (E) number and (F) area of adipocytes in SC, G and Mes fat of control diet fed cKO and *fl/fl* mice at 16-weeks of age (n≥4). Data are presented as the mean ± S.E.M. Significance is denoted by *P<0.05, **P<0.01, ***P<0.001.

Supplementary Figure 5. The mRNA expression of brown adipose tissue-associated metabolic genes unchanged between high-fat diet fed cKO and *fl/fl* mice.

The brown fat mRNA expression of selected metabolic genes including (A) *Slc2a1*, (B) *Slc2a4*, (C) *Ucp1*, (D) *Ucp2*, (E) *Dgat1* (F) *Dgat2*, and (G) *Lpl* was analysed. mRNA values generated were normalised to the geometric mean of *Gapdh* and *β-actin* house-keeping genes. Data are presented as the mean ± S.E.M (n=4).

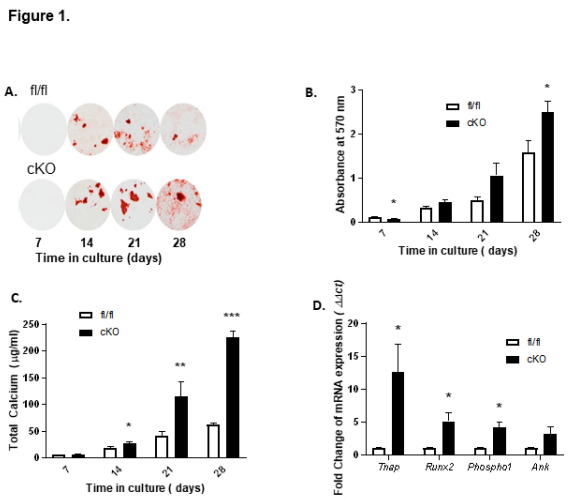

Figure 1. The matrix of Enpp1 deficient calvariae osteoblasts show a hypermineralized phenotype in vitro.

190x338mm (96 x 96 DPI)

Figure 2

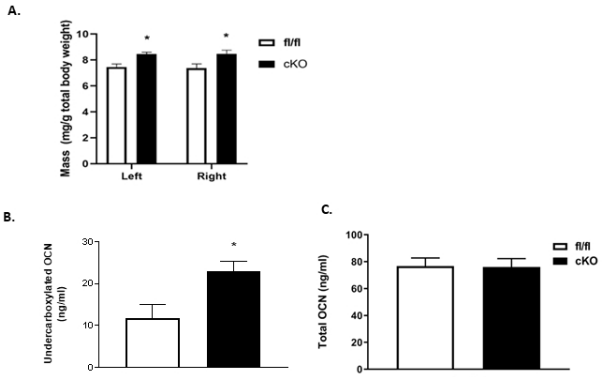

Figure 2. cKO mice display an altered quadriceps femoris mass and osteocalcin levels.

190x338mm (96 x 96 DPI)

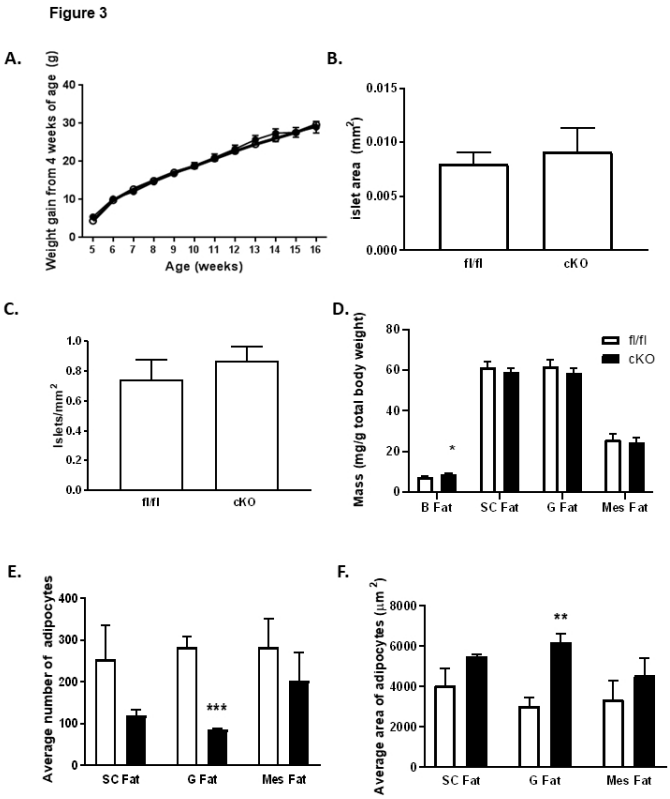

Figure 3. Assessment of pancreatic and fat tissue morphology in cKO and fl/fl male mice following a chronic HFD challenge.

190x338mm (96 x 96 DPI)

Figure 4

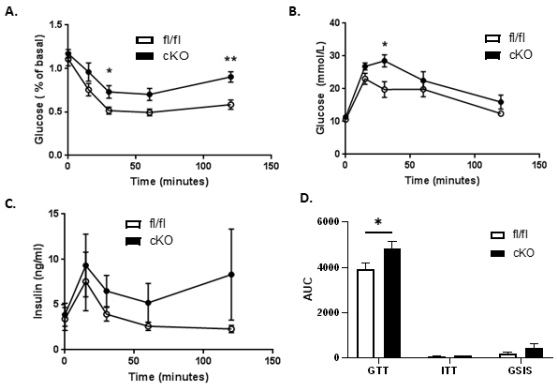

Figure 4. cKO mice show increased insulin resistance in response to a chronic HFD challenge.

190x338mm (96 x 96 DPI)